BNL-222645-2022-JAAM

An Automatic Processing Framework for In Situ Determination of Ecohydrological Root Water Content by Ground-Penetrating Radar

X. Liu, D. Yang

To be published in "IEEE Transactions on Geoscience and Remote Sensing"

March 2021

Environmental and Climate Sciences Department

Brookhaven National Laboratory

U.S. Department of Energy

USDOE Office of Science (SC), Biological and Environmental Research (BER) (SC-23)

DISCLAIMER

An Automatic Processing Framework for *In Situ* Determination of Ecohydrological Root Water Content by Ground-Penetrating Radar

Xinbo Liu, Li Gu, Xihong Cui, John R. Butnor, Elizabeth W. Boyer, Dedi Yang, Jin Chen, and Bihang Fan

***Abstract*— Root water content (RWC) is a vital component in water flux in soil–plant–atmosphere continuum. Knowledge of RWC helps to better understand the root function and the soil–root interaction and improves water cycle modeling. However, due to the lack of appropriate methods, field monitoring of RWC is seriously constrained. In this study, we used ground-penetrating radar (GPR), a common geophysical technique, to characterize RWC of coarse roots noninvasively. An automatic GPR data processing framework was proposed to (1) identify hyperbolic root reflections and locate roots in GPR images and (2) extract waveform parameters from the reflected wave of identified roots. These waveform parameters were then used to establish an empirical model and a semiempirical model to determine RWC. We validated the developed models using GPR root data at three antenna center frequencies (500 MHz, 900 MHz, and 2 GHz) that were produced from simulation experiments (with RWC ranging from 70% to 150%) and field experiments in sandy soils (with RWC ranging from 66% to 144%). Our results show that both the empirical and the semiempirical models achieved a good performance in estimating RWC with similar accuracy, i.e., the prediction error [root-mean-square error (RMSE)] was less than 8% for the simulation data and 12% for the field data. For both models, the accuracy of RWC estimation was the highest when applied to 2-GHz data. This study renders a new opportunity to determine RWC under field conditions that enhances the application of GPR for root study and the understanding and modeling of ecohydrology in the rhizosphere.**

***Index Terms*— Geophysics, ground-penetrating radar (GPR), model fitting, noninvasive, root ecology, waveform parameters.**

Manuscript received January 3, 2021; revised February 9, 2021; accepted March 5, 2021. Date of publication March 25, 2021; date of current version December 13, 2021. This work was supported in part by the National Natural Science Foundation of China under Grant 41401378 and Grant 41571404, and in part by the "Fundamental Research Funds for the Central Universities" at Sichuan University under Grant YJ202087 and Grant YJ202093. The work of Dedi Yang was supported by the United States Department of Energy to Brookhaven National Laboratory under Contract DE-SC0012704. *(Corresponding author: Bihang Fan.)*

Xinbo Liu, Xihong Cui, and Jin Chen are with the Faculty of Geographical Science, Beijing Normal University, Beijing 100875, China (e-mail: lxb@mail.bnu.edu.cn; cuixihong@bnu.edu.cn; chenjin@bnu.edu.cn).

Li Guo and Bihang Fan are with the State Key Laboratory of Hydraulics and Mountain River Engineering, College of Water Resource and Hydropower, Sichuan University, Chengdu 610065, China (e-mail: liguo01@scu.edu.cn; fanbh@scu.edu.cn).

John R. Butnor is with USDA Forest Service, Southern Research Station, 81 Carrigan Drive, Aiken Center, University of Vermont, Burlington, VT 05405 USA (e-mail: john.butnor@usda.gov).

Elizabeth W. Boyer is with the Department of Ecosystem Science and Management, Penn State University, University Park, PA 16801 USA (e-mail: ewb100@psu.edu).

Dedi Yang is with the Department of Ecology and Evolution, Stony Brook University, Stony Brook, NY 11794 USA, and also with the Environmental and Climate Sciences Department, Brookhaven National Laboratory, Upton, NY 11973 USA (e-mail: dediyang@bnl.gov).

I. Introduction

As a direct linkage between above- and belowground worlds, roots are crucial to both plant individuals and terrestrial ecosystems. Roots serve a variety of functions, including the absorption and storage of nutrients, water transport and uptake, and other biogeochemical processes in the ecosystem carbon budget [1]–[3]. Knowledge of root water content (RWC) is key to a comprehensive understanding of root functions and ecohydrological modeling of water movement between above- and belowground ecosystems [4], [5]. Moreover, RWC is a critical indicator of root physiological activity that influences gradients in water potential and drives water flux through the soil–plant–atmosphere continuum [6]. For example, the change in RWC can significantly affect root tensile strength, the transport of water, and nutrients toward root xylem vessels, and microbial respiration during the decomposition of plant litter [7]–[10]. Additionally, a recent study has used RWC as a wet-to-dry-mass conversion factor to yield global underground wet mass [11].

Despite the importance of roots, traditional methods for *in situ* root investigation are, however, destructive and labor-intensive, e.g., excavation and soil coring, limiting the repeatability of field sampling over a large area [12]. For example, root samples need to be excavated from the soil and taken back to the lab for oven drying to measure RWC [13]. This estimation procedure does not allow for the dynamic monitoring of RWC in natural settings. Therefore, practical measurements of RWC in the field, especially noninvasively and repeatedly, are seriously constrained so far.

Ground-penetrating radar (GPR) is a common noninvasive geophysical technique with the advantage of simple operation, high mobility, and rapid data collection over large areas [14]–[16]. Since its first application in root study in the 1990s, GPR has been successfully used to characterize a variety of root parameters, mainly for coarse roots (diameter $>$ 5 mm), such as root location, root distribution, and root system architectures as well as root diameter and biomass [17]–[20].

A standard GPR system is equipped with a pair of transmitter and receiver antennas placed at the ground surface for mapping subsurface objects [21]. The transmitter generates short pulses of high-frequency electromagnetic waves at a specific frequency (typically ranging from 250 MHz to 2.6 GHz) into the subsurface. The receiver collects the reflected wave from detected objects, e.g., roots, as a function of time. The reflected wave generation mainly depends on the contrast in the dielectric permittivity between the object root and surrounding soil [22]. The waveform parameters of the reflected wave are closely associated with root properties, e.g., root depth, root diameter, and RWC [19]. Previous studies have correlated various waveform parameters to root diameter and root biomass (see [21], [23]–[25]). For example, Barton and Montagu [22] estimated root diameter by using the time interval between two zero-crossings of the reflected wave (i.e., a time-related waveform parameter). Dannoura *et al.* [26] and Hirano *et al.* [13] examined the empirical linear relationship between coarse root biomass and the amplitude of the maximum reflected wave (i.e., a strength-related waveform parameter). After compensating radar energy attenuation with the penetrating depth, Cui *et al.* [27] used the high amplitude area of the reflected wave (i.e., a combination of strength- and time-related waveform parameters) to estimate root biomass of coarse roots at different depths.

Later, Guo *et al.* [28] demonstrated a considerable impact of RWC on root biomass estimation by GPR, especially when using the strength-related waveform parameters. According to the dielectric mixing theory, a root can be considered a complex of air, wood cellular material, and water [29]. Given that the permittivity of water ($\sim$81) is much larger than that of air ($\sim$1) and wood cellular materials ($\sim$4.5), RWC is likely the dominant factor controlling the dielectric permittivity of a root and, thus, the permittivity contrast between a root and the surrounding soil [30], [31]. The higher the RWC, the stronger the reflected wave is produced by a root under the same soil condition and root depth [28]. However, despite the nominal strong correlation between RWC and the strength of the GPR reflected wave of a root [13], [28], no study has tested the utility of GPR for quantifying RWC. This can be partly attributed to the complexity in establishing the numerical relationship between RWC and the strength-related waveform parameters since additional root parameters can also influence the strength of the reflected wave of a root [19], [32].

To link waveform parameters to a specific root parameter (e.g., root diameter and root biomass), previous studies have developed several forms of empirical regression models at different sites around the world [22], [23], [27], [33]. These empirical regression models are often established in a linear form based on the assumption that the waveform parameter used in models is controlled by a single root parameter to be estimated [28]. The inadequate consideration of the effects from multiple root parameters in the estimation models can lead to high uncertainty in model accuracy across study sites and even unsuccessful applications [19]. Further, uncertainty associated with waveform parameters also impacts model accuracy. For instance, extracting waveform parameters often depends on manual interpretation of root reflections in GPR images, which highly relies on the operator's experience [32]. Therefore, establishing an automatic data processing framework can reduce bias and promote the efficiency of root quantification with GPR in large-area investigations.

Recently, an increasing number of studies have related GPR waveform parameters to the water content of aboveground woody organs of plants, such as wood logs and tree trunks (see [34]–[37]). These studies demonstrated the validity of the GPR technique for water content determination in woody biomass, although such GPR measurements were conducted aboveground and not affected by soils. Therefore, we hypothesize that the GPR method can render an effective way to quantify RWC under field conditions, with the further advancement in the methodology of applying GPR to investigate roots (e.g., with an automatic data processing technique that extracts waveform parameters from root reflections, and numerical models that fully account for the influence of different root properties on waveform parameters).

The objective of this study is to quantify RWC noninvasively using GPR. Our specific goals are as follows:

1) to propose an automatic processing framework for extracting waveform parameters from the GPR reflected wave of a root.
2) to establish GPR-based RWC estimation models (hereinafter referred to as GPR-based RWC models) that link waveform parameters to RWC.
3) to compare different GPR-based RWC models in quantifying RWC.

To the best of our knowledge, this is the first study to evaluate the use of GPR for determining RWC. The rest of this article is organized as follows. Section II introduces the field and simulation experiments for GPR data collection. Section III describes the automatic processing framework and the establishment of GPR-based RWC models. Sections IV and V present the evaluation methods and the results for the GPR-based RWC models, respectively. Section VI discusses the limitation and outlooks of the proposed method, and Section VII provides concluding points.

II. Field and Simulation Experiments

A. Experimental Site

The field-controlled experiment was conducted in the southern part of Hunshandak Sandy Land (42°26′ N and 116°11′ E), Inner Mongolia, China (Fig. 1). This area has a temperate semiarid climate, with an annual mean temperature of 1.6 °C and annual precipitation of 386 mm [38]. The landscape of the study area features fixed sand dunes (Fig. 1). The vegetation cover is dominated by shrub colonies such as *Caragana microphylla*, *Ulmus pumila*, *Artemisia ordosica*, *Stipa glareosa*, and *Poa annua* [39]. The local soil is dry sandy soil with 95% sand, 2% silt, and 3% clay, and the average soil water content (SWC) is around 0.105 $m^3 \cdot m^{-3}$ [27]. The soil is relatively homogeneous without obvious soil horizonation and macropore structures, which may interfere with the detection of roots in GPR images, and hence favors the application of GPR to measure roots.

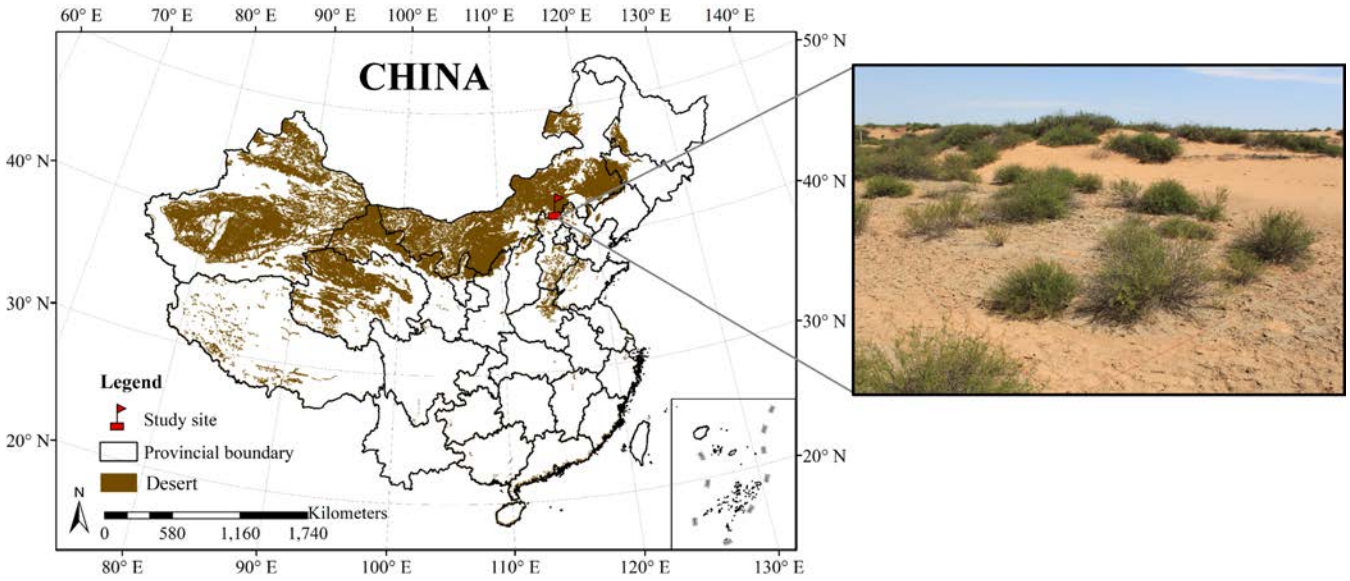

Fig. 1. (Left) Location of the experimental site. The base map depicts the distribution of desert in China, which is distributed by the Environmental & Ecological Science Data Center for West China, Lanzhou, Gansu, China (http://westdc.westgis.ac.cn). (Right) Photograph of *Caragana microphylla* colonies distributing on sand dunes in the study area.

B. Root Samples

Root systems of five shrub individuals (*Caragana microphylla*) were excavated at the study site (Fig. 1). A total of 20 coarse root samples, which were relatively straight with minimal tapering and cut to the same length of 0.7 m, were retained for GPR measurement. Fresh weights and diameters of root samples were measured immediately after excavation (Table I). The prepared root samples were grouped into five levels with an approximate diameter of 10, 15, 20, 25, and 35 mm, respectively (Table I).

Molten wax was used to seal the cut ends of root samples to limit water loss from roots during the field experiments. These root samples were then buried in the soil as reflectors for GPR data collection. After field experiments, all root samples were taken to the laboratory and oven-dried at 65 °C until constant root weights were reached to measure the dry weights and, further, the gravimetric RWC of root samples (i.e., the ratio of root water mass to root dry weight). The selected root samples created a gravimetric RWC gradient from 80.28% to 144.01% (Table I). It is noted that the RWC indicated in this article is gravimetric RWC.

C. Root GPR Data Collection in the Field

Five soil trenches (each with 4.2 m length, 1.2 m width, and 1.0 m depth) were dug at a relatively flat area at the study site. Perpendicular to each soil trench wall, four holes with a horizontal interval of 1.0 m were drilled at a depth of 0.2, 0.3, 0.4, and 0.6 m, respectively, to bury root samples [Fig. 2(a)]. The inlet length of each hole was 0.8 m so that root samples could be fully inserted into the soil. Root samples from the same diameter group (e.g., root sample No. 1, 6, 11, and 16, representing roots with a diameter of 10 mm) were inserted into the same soil trench at four depths [Fig. 2(a)]. Then the soil trench was refilled, and the surface was flattened before GPR measurements. This experimental setup ensured a minimal disturbance to the original soil above root samples [27].

A field-portable GPR system, Zond–12e (Georadar Systems Inc., Riga, Latvia), equipped with three shielded antenna pairs at the center frequency of 500 MHz, 900 MHz, and 2 GHz (i.e., the common GPR frequencies for root investigation) was employed to scan the roots. First, three GPR survey lines with a spacing of 10 cm were laid out perpendicular to the long axis of the root samples [Fig. 2(b)]. Then the GPR system was dragged over the buried root samples along the predesigned survey lines [Fig. 2(b)]. Then we changed the antenna pairs to repeat GPR data collection until root samples were scanned at all three antenna center frequencies.

D. Forward Simulation

To complement field experiments with limited root samples, a set of simulations was performed to generate GPR root reflection data under various levels of RWC, root diameters, and GPR antenna center frequencies. All simulations were completed with the GprMax V2.0, an open-source software [40] that has been used in GPR root signal simulation in various studies [41]–[43].

The GprMax simulator generates GPR images with root reflections based on input information of antenna center frequency, the electromagnetic attributes of the soil and object roots, and the relative position of roots and the surrounding soil [29], [42]. In our simulations, soil texture was set to sand with a dielectric permittivity of 5.53, calculated according to Topp's equation using SWC at 0.105 $m^3 \cdot m^{-3}$ [44]. The root depth was set to 0.3 m and the geometric domain of the soil was set to 1.2 m wide and 0.8 m deep (Fig. 3). Each simulated GPR image was composed of 54 A-scans (i.e., radar traces), and the time window of each A-scan was set to 20 ns. Considering both numerical stability and model

TABLE I

ROOT PARAMETERS AND GPR ROOT DETECTION RESULTS FOR ROOT SAMPLES SELECTED IN THE FIELD EXPERIMENT. THE CIRCLE MARKERS REPRESENT THAT ROOT SAMPLES ARE DETECTED BY GPR WHEREAS THE CROSS MAKERS REPRESENT THAT ROOT SAMPLES ARE NOT DETECTED

Root sample No.	Root parameters					Visible root detection		
	Depth (m)	Diameter (mm)	Fresh weight (g)	Dry weight (g)	Gravimetric RWC (%)	500 MHz	900 MHz	2 GHz
1		11.60	67.00	33.00	103.03	×	○	○
2		17.66	128.00	71.00	80.28	○	○	○
3	0.2	21.34	200.50	94.20	112.85	○	○	○
4		25.59	349.00	148.90	134.39	○	○	○
5		37.55	656.00	317.00	106.94	○	○	○
6		10.36	45.20	20.70	118.36	×	○	○
7		15.34	120.50	56.00	115.18	○	○	○
8	0.3	22.25	210.40	91.00	131.21	○	○	○
9		26.6	358.80	150.20	138.88	○	○	○
10		33.66	547.10	231.40	136.43	○	○	○
11		11.66	57.20	24.50	133.47	×	○	○
12		17.10	138.90	69.20	100.72	○	○	○
13	0.4	21.97	211.80	86.80	144.01	○	○	○
14		24.88	291.10	137.20	112.17	○	○	○
15		39.03	681.70	305.80	122.92	○	○	○
16		11.48	58.30	31.80	83.33	×	○	×
17		15.05	115.80	55.70	107.90	○	○	○
18	0.6	19.36	162.00	76.50	111.76	○	○	○
19		24.23	263.70	114.00	131.32	○	○	○
20		37.27	640.40	288.40	122.06	○	○	○

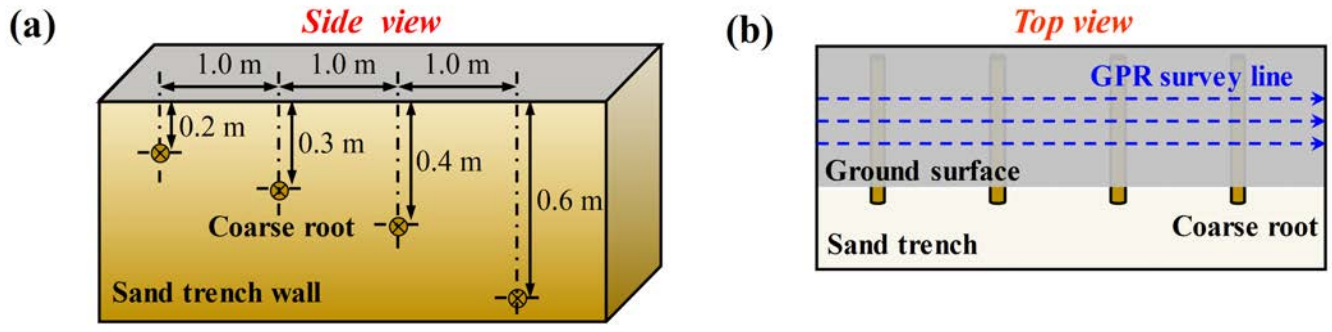

Fig. 2. Schematic of the field experiment for collecting GPR root reflection data. (a) Side view of a soil trench and (b) top view of three GPR survey lines on the ground surface.

reliability, the spatial discretization of the geometric domain in simulations was set to 2.5 mm.

According to an extensive investigation of RWC of shrub species in the study region [28], nine gravimetric RWC levels (from 70% to 150% with an increment of 10%) were included in the simulations, together with nine root diameter levels (from 10 to 50 mm with an increment of 5 mm) to represent common shrub root conditions at the study site. To be consistent with the field experiments, three antenna center frequencies (e.g., 500 MHz, 900 MHz, and 2 GHz) were

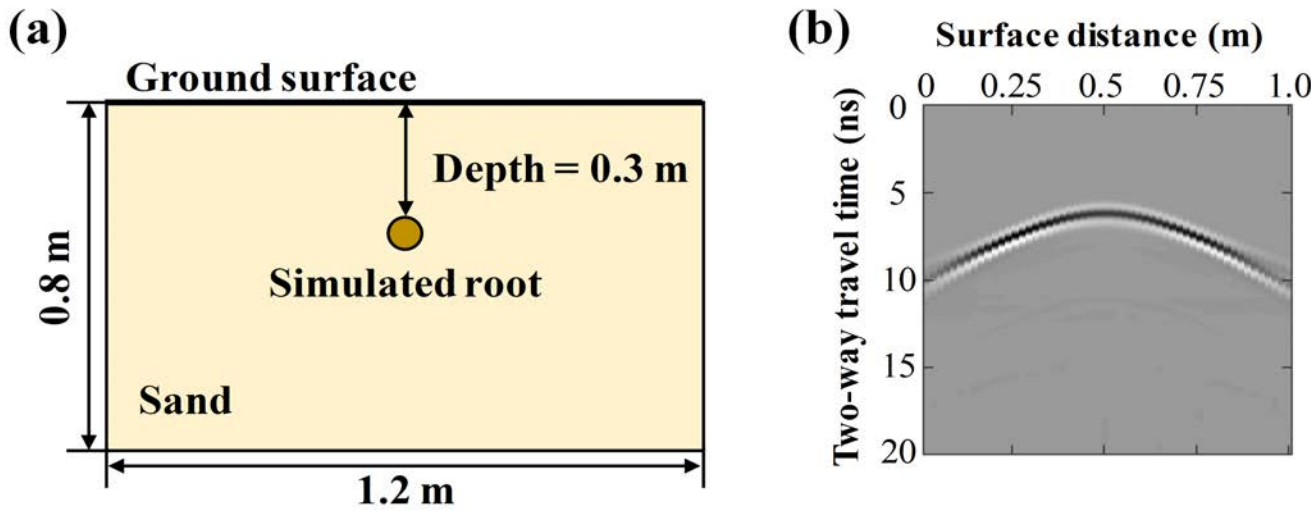

Fig. 3. (a) Geometric domain for all simulations. (b) Example of a simulated GPR image with a root reflection, i.e., the hyperbolic reflection. Root diameter was set to 20 mm, RWC 110%, antenna center frequency 900 MHz, and SWC 0.105 $m^3 \cdot m^{-3}$.

selected for simulations. Therefore, a total of 243 GPR images with root reflections (i.e., 9 RWC levels × 9 root diameter levels × 3 antenna frequencies) were generated [Fig. 3(b)].

III. Automatic Processing Framework for GPR-Based RWC Estimation

This section proposes an automatic GPR data processing framework in combination with GPR-based RWC models to determine RWC (Fig. 4):

1) preprocessing raw GPR images to enhance the signal-to-noise ratio and the detection of hyperbolic reflections of roots.
2) automatically identifying hyperbolic reflections to locate roots in preprocessed GPR images and extract waveform parameters of root reflections.
3) establishing GPR-based RWC models using extracted waveform parameters in 2) to get a measure of RWC.

A. GPR Data Preprocessing

Raw GPR images require several preprocessing procedures to extract waveform parameters accurately, including zero-time correction, background removal, and amplitude compensation [19]. The zero-time correction shifts the radar signal to start from the ground surface, ensuring accurate locating of roots [45]. Background removal eliminates noises to facilitate the identification of root reflections in GPR images [46]. Amplitude compensation calibrates energy attenuation of GPR reflected wave with penetrating depth so that the strength of root reflections is independent of depth [27]. Fig. 5 exhibits examples of GPR images before and after preprocessing, which depicts a clear hyperbolic reflection.

B. Automatic Extraction of Waveform Parameters

The proposed method achieves the automatic extraction of waveform parameters of a root reflection via three steps (Fig. 5).

1) An image edge extraction operator, the Sobel filter, was performed on the preprocessed GPR image [32]. Then, the gray-scale GPR image was converted into a binary image [Fig. 5(c)]. Each connected edge in the binary GPR image was considered the region of interest (ROI) of a hyperbola. Generating an ROI helps reduce the computational time in identifying hyperbolic root reflections in the following step.
2) The randomized Hough transform method, a widely used technique of identifying hyperbolic shapes [47], [48], was applied to each ROI [Fig. 5(c)]. Based on hyperbola parameter determination, the randomized Hough transform method identified an optimal hyperbola as a root reflection automatically [Fig. 5(d)]. The apex of the identified hyperbola was considered the root location [49], [50]. Details of using the randomized Hough transform method to identify root reflections can be found in Li *et al.* [32] and Liu *et al.* [41].
3) The A-scan passing through the root location on the identified root reflection was selected for extracting waveform parameters of the reflected wave of the detected root [Fig. 5(e)], including $A_{\max}$ (i.e., the maximum amplitude) and Δt (i.e., the time interval between two zero-cross points of t_1 and t_2). Further, $A_{\max}$ and Δt were used to calculate P_{area} (i.e., maximum amplitude area) of the reflected wave

$$P_{\text{area}} = \frac{1}{2} \times A_{\max} \times \Delta t. \tag{1}$$

C. Two GPR-Based RWC Models

Root depth, root diameter, and RWC are the primary root properties that control the signal strength of the reflected wave of a root in GPR images [19]. Given that data preprocessing conducted above has calibrated the impact of varying root depths on GPR signal strength, we assumed that the compensated signal strength positively correlates with root diameter

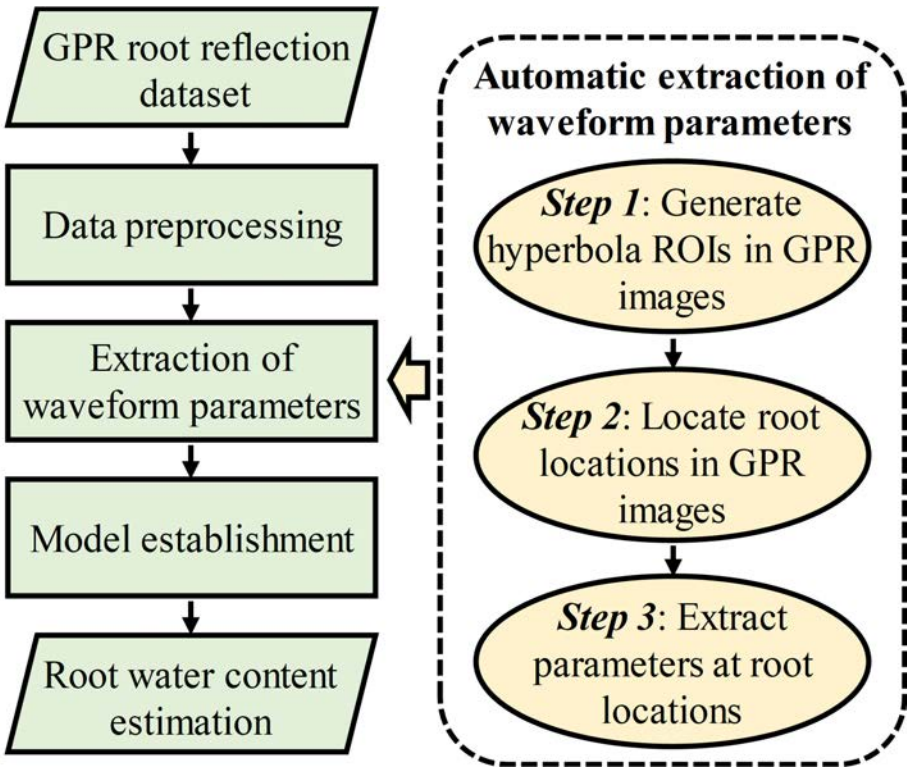

Fig. 4. Proposed automatic processing flowchart for RWC determination from GPR images. ROI refers to the region of interest of a hyperbolic reflection in GPR images.

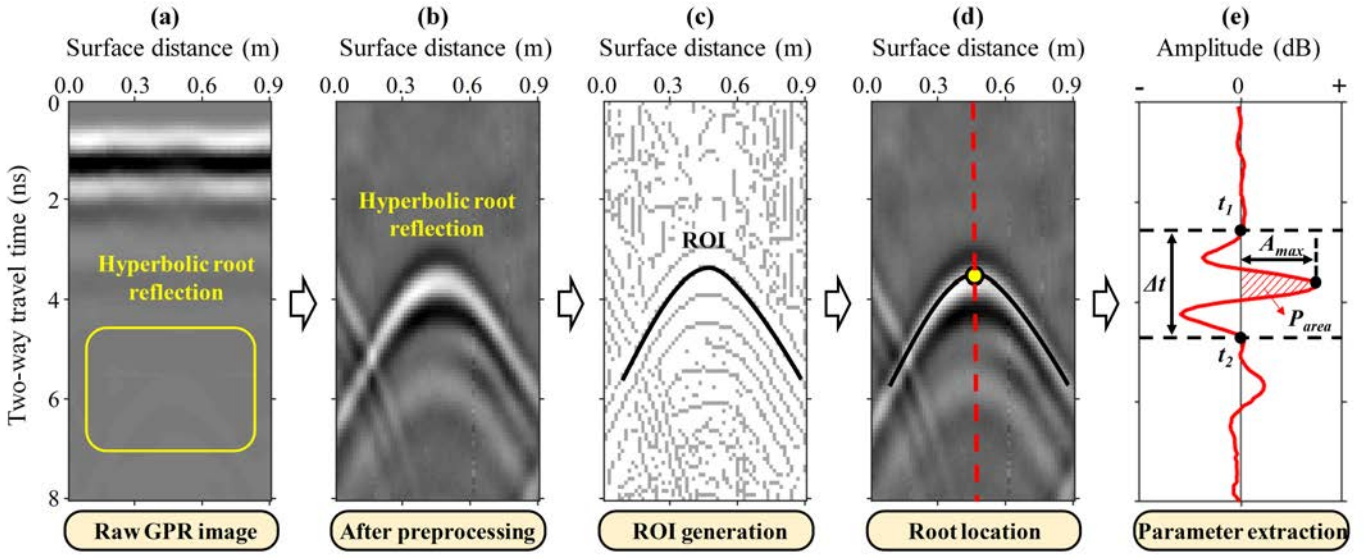

Fig. 5. Procedure of automatic extraction of waveform parameters from a hyperbolic reflection of a root. (a) Raw GPR image was collected by a 900-MHz antenna, showing a blurry hyperbolic reflection formed by a root (indicated in the yellow box). (b) Corresponding GPR image after preprocessing. (c) Binary GPR image after edge extraction. Each connected edge (indicated by the solid curve) refers to the ROI. (d) Apex of the hyperbola (indicated by the yellow dot) indicates the location of the detected root. (e) A-scan [indicated by the red dashed line in (d)] passing through the root was selected for extracting waveform parameters of the reflected wave (indicated by the red curve), including time interval (Δt), maximum amplitude ($A_{\max}$), and maximum amplitude area (P_{area}).

and RWC only (Fig. 6). Existing studies usually correlated a root property (root diameter or root biomass) to root's GPR signal strength via linear regression models [13], [22], [28]. However, as shown in Fig. 6, different root diameters shift the linear relationship between RWC and the signal strength. Therefore, we proposed two ways to characterize the relationship between RWC and signal strength with the consideration of root diameter.

One way is to develop multivariate regression

$$\text{RWC} = a_1 \times S + b_1 \times D + c_1 \times S \times D + d_1 \quad (2)$$

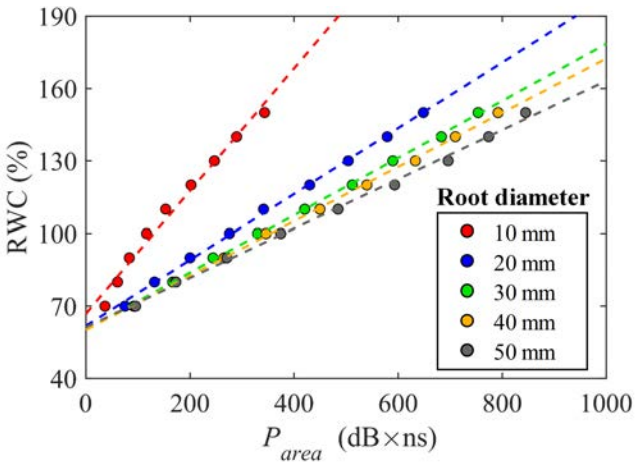

Fig. 6. Change in P_{area} along RWC gradient at different levels of root diameter. The values of P_{area} were extracted from GPR images simulated at 900 MHz following the method detailed in Section II-D. Dashed lines depict the linear relationship between RWC and P_{area}.

where S is the signal strength of GPR root reflections, D is root diameter, and a_1, b_1, c_1, and d_1 are unknown parameters that can be determined by fitting the models to a set of values of S and D. Equation (2) is considered an empirical model because RWC is directly linked to signal strength and root diameter by a nonlinear regression model.

The other way accounts for GPR reflection principles

$$\text{RWC} = \frac{1}{a_2 \times D + b_2} \times S + c_2 \tag{3}$$

where a_2, b_2, and c_2 are unknown parameters. In (3), $1/(a_2 \times D + b_2) \times S$ can be conceptualized as the signal strength generated by per unit root diameter, which varies with different values of RWC. Moreover, $1/(a_2 \times D + b_2)$ represents the slope of the linear relationship between RWC and root's GPR signal strength, i.e., the larger the root diameter, the smaller the slope. This trend is consistent with the theoretical simulation results (Fig. 6), indicating that the relative contribution to root's GPR signal strength by RWC decreases at greater root diameter levels. As it is rooted in the physical principles of GPR reflection generation, (3) is considered a semiempirical model.

To solve the models, we used different sets of waveform parameters to determine S and D, respectively. Since Δt has been proven closely related to D with a linear relationship [22], [51] (refer to Fig. 10), we used Δt as a surrogate of D. Moreover, we used P_{area} as a surrogate of S because P_{area} is a robust waveform parameter representing the signal strength and strongly correlated with RWC [13], [24], [27], [28].

IV. Model Evaluation

A. Data Preparation

The simulated data were divided into two groups, the training data and the testing data, both with the same range of RWC from 70% to 150%. The training data were used to fit model parameters and evaluate mode fitting at five root diameter levels (i.e., 10, 20, 30, 40, and 50 mm). The testing data were used to assess the models' performance in estimating RWC at the other four root diameter levels (i.e., 15, 25, 35, and 45 mm). Thus, for each GPR frequency, the training data consisted of 45 simulated GPR images while the testing data consisted of 36 simulated GPR images. The purpose of using a bigger portion of the data set for model training is to capture a wider variation of the data and thus make the models more robust for prediction.

For the field experiment, different antenna center frequencies displayed varied abilities in detecting root samples (Table I). The 500-MHz GPR antenna detected 16 root samples but could not detect four root samples at the 10-mm-diameter level due to the low detection resolution. The 2-GHz GPR antennas detected 19 root samples but failed to detect the root sample with the 10-mm root diameter at 0.6 m depth due to the limited detection depth. In contrast, the 900-MHz GPR antenna detected all 20 root samples, providing the best combination of detection depth and resolution. To compare models at different antenna center frequencies, we only used GPR data collected from 16 root samples that were detected at any selected frequency (Table I) to fit models and evaluate model fitting. Then due to the limited number of root samples, we carried out the leave-one-out cross validation (LOOCV) on data collected from 16 root samples to assess model performance in estimating RWC.

B. Model Fitting Assessment

To examine whether the established models are statistically significant in representing the relationships between variables, we evaluated the fit of the models to training data in three aspects, (1) the F value (F_{value}) from an F test to reflect the overall significance of the fit of the models, (2) the coefficient of determination (R^2) and the adjusted R^2 (R^2_{adjusted}) to evaluate the goodness of the fit of the model,; and (3) the square root of the variance of the residuals (S_{r}) to characterize the precision of the fit of the models [52]

$$F_{\text{value}} = \frac{\sum_{k=1}^{m}\left(\text{RWC}_k^{\text{estimated}} - \overline{\text{RWC}}^{\text{fitting}}\right)^2}{\sum_{k=1}^{m}\left(\text{RWC}_k^{\text{fitting}} - \text{RWC}_k^{\text{estimated}}\right)^2} \times \frac{(m-p)}{(p-1)} \tag{4}$$

$$R^2 = 1 - \frac{\sum_{k=1}^{m}\left(\text{RWC}_k^{\text{fitting}} - \text{RWC}_k^{\text{estimated}}\right)^2}{\sum_{k=1}^{m}\left(\text{RWC}_k^{\text{fitting}} - \overline{\text{RWC}}^{\text{fitting}}\right)^2} \tag{5}$$

$$R^2_{\text{adjusted}} = 1 - \frac{\sum_{k=1}^{m}\left(\text{RWC}_k^{\text{fitting}} - \text{RWC}_k^{\text{estimated}}\right)^2}{\sum_{k=1}^{m}\left(\text{RWC}_k^{\text{fitting}} - \overline{\text{RWC}}^{\text{fitting}}\right)^2} \times \frac{(m-1)}{(m-p)} \tag{6}$$

and

$$S_r = \sqrt{\frac{\sum_{k=1}^{m}(\text{RWC}_k^{\text{fitting}} - \text{RWC}_k^{\text{estimated}})^2}{m-p}} \tag{7}$$

where $\mathrm{RWC}_k^{\mathrm{estimated}}$ is the model-estimated RWC value for the kth root sample and $\mathrm{RWC}_k^{\mathrm{fitting}}$ is the RWC value of the kth root sample that was used to fit the model. $\overline{RWC}^{\mathrm{fitting}}$ is the mean value of the RWC of m root samples. m is the number of root samples used for fitting the models, i.e., 45 for the simulation training data and 16 for the field data, and p is the number of model parameters, with 4 for the empirical model [see (2)] and 3 for the semiempirical model [see (3)]. The F values were calculated to compare with F critical values at the 0.01 significance level from the F distribution table. Given that adding variables to the prediction models can increase R^2 values, the R^2_{adjusted} was also calculated to compare model fitting.

C. Assessing the Accuracy of RWC Estimation by Proposed Models

Four statistical metrics were calculated to compare RWC estimated by the proposed models to actual values, including root-mean-square error (RMSE), correlation coefficient (r), relative error (RE), and the mean absolute error (MAE), as shown at the bottom of the page no. 10, and

$$\mathrm{MAE} = \frac{1}{N} \times \sum_{i=1}^{N} \left| \mathrm{RWC}_i^{\mathrm{estimated}} - \mathrm{RWC}_i^{\mathrm{actual}} \right| \qquad (11)$$

where $\mathrm{RWC}_i^{\mathrm{estimated}}$ and $\mathrm{RWC}_i^{\mathrm{actual}}$ are model-estimated and actual RWCs for the ith root sample, respectively. $\overline{\mathrm{RWC}}^{\mathrm{estimated}}$ and $\overline{\mathrm{RWC}}^{\mathrm{actual}}$ are the average of model-estimated and actual RWCs for all N root samples, respectively. N is the total number of root samples for comparing model accuracy, with 36 for the simulation testing data and 16 for the field data. RMSE and r were used to evaluate the prediction precision and degree of agreement between model-estimated and actual RWC, respectively. Given the complex influence of multiple environmental factors on field data, RE and MAE were only computed for the simulation data to analyze the influence of RWC and root diameter on the proposed models' accuracy.

V. Results

A. Model Fitting

For the simulation training data, all models show a high value of R^2 (>0.85), regardless of different GPR frequencies (Table II). Moreover, all models fit the training data well, and the goodness of the fit of models is statistically significant, with the F_{value} values larger than the corresponding F critical values (i.e., f_{value} in Table II) at the 0.01 significance level. Further, the precision of these fit models ranges from 6.54% to 8.87% (i.e., S_{r} in Table II). Thus, the proposed models are effective at quantitatively describing the relationship between RWC and waveform parameters.

Both models are also fit well to the field GPR data at three antenna center frequencies, with R^2 values larger than 0.68 and F_{value} values passing F test (Table II). Nevertheless, the precision of the models fit to the field data is slightly lower than that fit to the simulation data, ranging from 9.50% to 12.43% (Table II). When 2-GHz data are used, both models achieve the highest R^2_{adjusted} and F_{value}. Hence, the proposed models are best fit to the GPR data at a higher antenna center frequency (Table II).

B. RWC Estimations With Two GPR-Based RWC Models

Fig. 7 shows the application results of the proposed GPR-based RWC models to the simulation testing data. All models established for varied frequency data achieve a good performance in estimating RWC, with the maximum RMSE of less than 7.94% and the minimum r greater than 0.96 [Fig. 7(e)]. Both models established for the 2-GHz data produce the best estimation accuracy of RWC, with an RMSE value of 6.16% (or 6.34%) and an r value of 0.97 (or 0.97) for the empirical model (or the semiempirical model) [Fig. 7(c) and (f)]. Moreover, the narrow ranges of RMSE and r values indicate that the overall performance of proposed models is relatively consistent in estimating RWC.

Results of using GPR-based RWC models established for the field data to estimate RWC are shown in Fig. 8. Regardless of GPR frequency, both models exhibit good and stable performance in estimating RWC, with RMSE values ranging from 8.57% to 11.21% and r values ranging from 0.75 to 0.85 (Fig. 8). The semiempirical model established using the 2-GHz data achieves the lowest RMSE and the highest r [Fig. 8(f)], whereas the models established using data collected at lower antenna center frequencies result in higher RMSE values and lower r values, i.e., a lower accuracy in estimating RWC [Fig. 8(a) and (d)].

In all, the proposed empirical and semiempirical models are capable of achieving a reasonable estimation of RWC regardless of antenna center frequencies. In terms of RMSE and r (Figs. 7 and 8), the empirical model slightly outperforms the semiempirical model in estimating RWC in most cases. Both models established using 2-GHz data achieve more accurate estimations of RWC than using data obtained at a lower frequency.

C. Impacts of RWC and Root Diameter on the Performance of the GPR-Based RWC Models

Fig. 9 confirms that REs and MAEs vary at different RWCs and root diameters. By comparing Fig. 9(a)–(c) to Fig. 9(d)–(f), the change in MAEs with root diameter is similar between the empirical and semiempirical models but divergent among antenna center frequencies. This suggests that the impacts of root diameter on RWC estimation are more sensitive to antenna center frequency than to the model forms. In contrast, according to the comparison between Fig. 9(a)−(d) to Fig. 9(b)−(e), the impacts of RWC levels on RWC estimations are more sensitive to the form of the models, especially for RWC estimation using data at 500 and 900 MHz. For RWC estimation using data at 2 GHz [Fig. 9(c) and (f)], the impacts of both root diameter and RWC levels on the accuracy of RWC estimation show no noticeable difference between model types. Regardless of antenna center frequency, the semiempirical model exhibits a higher accuracy of RWC estimation at lower RWC levels from 70% to 100% [Fig. 9(a)–(c)] whereas the empirical model displays a higher accuracy of RWC estimation at higher RWC levels from 100% to 150% [Fig. 9(d)−(f)].

TABLE II

F VALUE (F_{value}), COEFFICIENT OF DETERMINATION (R^2), SQUARE ROOT OF THE VARIANCE OF THE RESIDUALS (S_r), AND PARAMETERS OF TWO GPR-BASED RWC MODELS FIT TO THE SIMULATION AND FIELD GPR DATA AT THREE GPR FREQUENCIES. THE BOLD ITALICIZED NUMBERS REFER TO THE NUMBER OF ROOT SAMPLES INVOLVED IN FITTING MODELS. THE f_{value} REFERS TO THE F CRITICAL VALUE AT THE 0.01 SIGNIFICANCE LEVEL FROM THE *F* DISTRIBUTION TABLE

Parameters	Forward simulation data			Field data		
	500 MHz (***45***)	900 MHz (***45***)	2 GHz (***45***)	500 MHz (***16***)	900 MHz (***16***)	2 GHz (***16***)
Empirical model (Equation (2))						
R^2	0.85	0.90	0.93	0.76	0.84	0.84
$R^2_{adjusted}$	0.84	0.89	0.92	0.70	0.80	0.80
F_{value}	124.27	128.21	198.46	8.76	11.25	11.38
f_{value}	4.31	4.31	4.31	5.59	5.59	5.59
S_r	7.45%	7.73%	6.54%	11.85%	10.15%	11.44%
a_1	0.14	0.14	0.30	0.07	0.21	0.45
b_1	-112.00	-55.20	-13.50	29.99	47.07	44.82
c_1	0.002	0.0009	-0.04	-0.02	-0.06	-0.21
d_1	456.20	194.60	75.41	-28.33	-49.04	7.46
Semi-empirical model (Equation (3))						
R^2	0.88	0.91	0.94	0.70	0.80	0.83
$R^2_{adjusted}$	0.87	0.90	0.93	0.66	0.76	0.80
F_{value}	179.60	153.10	193.46	11.72	16.47	21.57
f_{value}	5.18	5.18	5.18	6.70	6.70	6.70
S_r	7.95%	8.87%	6.62%	12.43%	10.14%	9.50%
a_2	13.85	7.93	2.00	17.32	6.09	14.84
b_2	-43.35	-12.75	1.20	10.11	7.53	-13.56
c_2	55.84	58.94	53.59	82.95	75.98	83.41

Compared with RWC estimations using 500- and 900-MHz data, RWC estimations using two GPR data achieve a higher accuracy regardless of model types [Fig. 9(c) and (f)].

VI. DISCUSSION

A. Applicability of the Proposed Framework

Results from both simulation and field data confirm the applicability of the GPR method for estimating RWC at different antenna center frequencies. However, due to the difference in the detection resolution and detection range (Table I), antenna center frequency significantly affects the performance of GPR-based RWC models (Figs. 7 and 9). Previous studies recognized the dependence of root detection on antenna center frequency [13], [19]. The field experiment in this study also showed that the 2-GHz GPR failed to detect the root at 0.6 m depth, and the 500-MHz GPR was unable to detect roots at the10-mm root diameter level (Table I). Given

the tradeoff between the detection resolution and penetrating depth, the 900-MHz GPR detected all roots and could achieve a reasonable accuracy of RWC estimation (Tables III and IV in the Appendix).

Different antenna center frequencies affect the identification of root reflections and hence the extraction of waveform parameters. For example, 2-GHz and 900-MHz data are more accurate than 400-MHz data to identify root reflections [32]. Further, the higher the GPR frequency, the more accurate the extraction of waveform parameters [27]. This also explains why the proposed two models performed the best when 2-GHz data were used (Figs. 7 and 8), especially at the root diameter level of 15 mm (i.e., the minimal root diameter levels) in the simulation experiment (Fig. 9).

Soil condition (e.g., soil water and clay content) also influences root detection by GPR [49]. For example, soil with high water content and/or high clay content seriously degrade the GPR's performance in measuring roots [25]. The higher the antenna center frequency, the more serious the degradation of GPR data quality in wet soil [12]. Recently, Cui *et al.* [53] found that GPR surveys detected more roots in winter than in summer, because SWC decreased from summer to winter and created a more considerable contrast in dielectric permittivity between roots and surrounding soils. Therefore, the performance of the proposed framework likely varies across study sites and periods.

B. Advantages of the Proposed Framework

Recent studies have noted the significance of automatic GPR data processing in locating root distribution [32], [53], mapping soil moisture in the root zone [54], and reconstructing root system structure [12]. The automatic processing framework proposed in this study further implements the extraction of waveform parameters from GPR root reflections and the quantification of RWC. Instead of the manual extraction of waveform parameters in previous studies (see [13], [23], [25], [28]), the proposed framework improves the efficiency of GPR data interpretation at larger areas and minimizes artificial bias.

Although the application of automatic GPR data processing and GPR-based root quantification have gained increasing attention [24], [32], only a few efforts have been pursued to combine the two aspects to measure roots automatically. This study integrates automatic GPR data processing and GPR-based RWC determination, which can be further refined to measure other root properties such as root diameters and root biomass. Due to the advantages of flexible mobilization and rapid data collection, GPR has been used for extensive root investigations over a large area [24], [54]–[56]. The automatic processing framework provides timely support to propel rapid interpretation of massive GPR root data sets, especially with the rise of big data applications for GPR [57]. In genetic research, the rise of automated interpretation of millions of data points greatly accelerated the field of genomics. Automated GPR analysis of multiple rhizosphere parameters could lead to a new quantitative study of roots, rooting zone, density, distribution, hydrology, and interaction with the environment called "rhizonomics" and change how difficult root–environment hypotheses are tested. With the further enhancement of automatic data processing, it is possible to develop real-time GPR measurements of variable root properties in the future.

C. GPR-Based RWC Determination

Root biomass is a key indicator for studying plant response to environmental change and soil carbon sequestration [58]. The impacts of RWC on root detection and root biomass quantification by GPR have been previously noted [13], [26], [28]. This study extends the application of GPR to measure RWC. It helps improve the accuracy of measuring root biomass by GPR by providing information about RWC, which creates an opportunity to calibrate the influence of RWC on root biomass measurement.

Different from previous GPR-based models for root biomass/diameter estimation, which mostly relied on a single GPR index (see [22], [23], [28], [33]), the GPR-based RWC models proposed here take into account the joint effects of multiple root properties (RWC and root diameter) on root GPR reflections. The good fitting and estimation accuracy of both empirical and semiempirical models confirm their feasibility in quantifying RWC (Table II, Figs. 7 and 8).

Compared with the empirical model, the semiempirical model has fewer unknown variables and is more efficient in the calculation [59]. Moreover, the semiempirical model offers a physical interpretation for each involved variable, which facilitates understanding of the underlying mechanism that governs the response of root GPR reflections to root properties. Although the overall accuracy of the semiempirical model is slightly lower than the empirical model in most study cases (Figs. 7 and 8), the consistent pattern of the model bias, i.e., high accuracy at low RWC but low accuracy at high RWC (Figs. 7 and 9) ensures a potential for further

$$\mathrm{RMSE} = \sqrt{\frac{1}{N} \times \sum_{i=1}^{N} \left(\mathrm{RWC}_i^{\mathrm{estimated}} - \mathrm{RWC}_i^{\mathrm{actual}}\right)^2} \tag{8}$$

$$r = \frac{\sum_{i=1}^{N} \left[\left(\mathrm{RWC}_i^{\mathrm{estimated}} - \overline{RWC}^{\mathrm{estimated}}\right) \times \left(\mathrm{RWC}_i^{\mathrm{actual}} - \overline{\mathrm{RWC}}^{\mathrm{actual}}\right)\right]}{\sqrt{\sum_{i=1}^{N} \left(\mathrm{RWC}_i^{\mathrm{estimated}} - \overline{\mathrm{RWC}}^{\mathrm{estimated}}\right)^2} \times \sqrt{\sum_{i=1}^{N} \left(\mathrm{RWC}_i^{\mathrm{actual}} - \overline{\mathrm{RWC}}^{\mathrm{actual}}\right)^2}} \tag{9}$$

$$\mathrm{RE}_i = \mathrm{RWC}_i^{\mathrm{estimated}} - \mathrm{RWC}_i^{\mathrm{actual}} \tag{10}$$

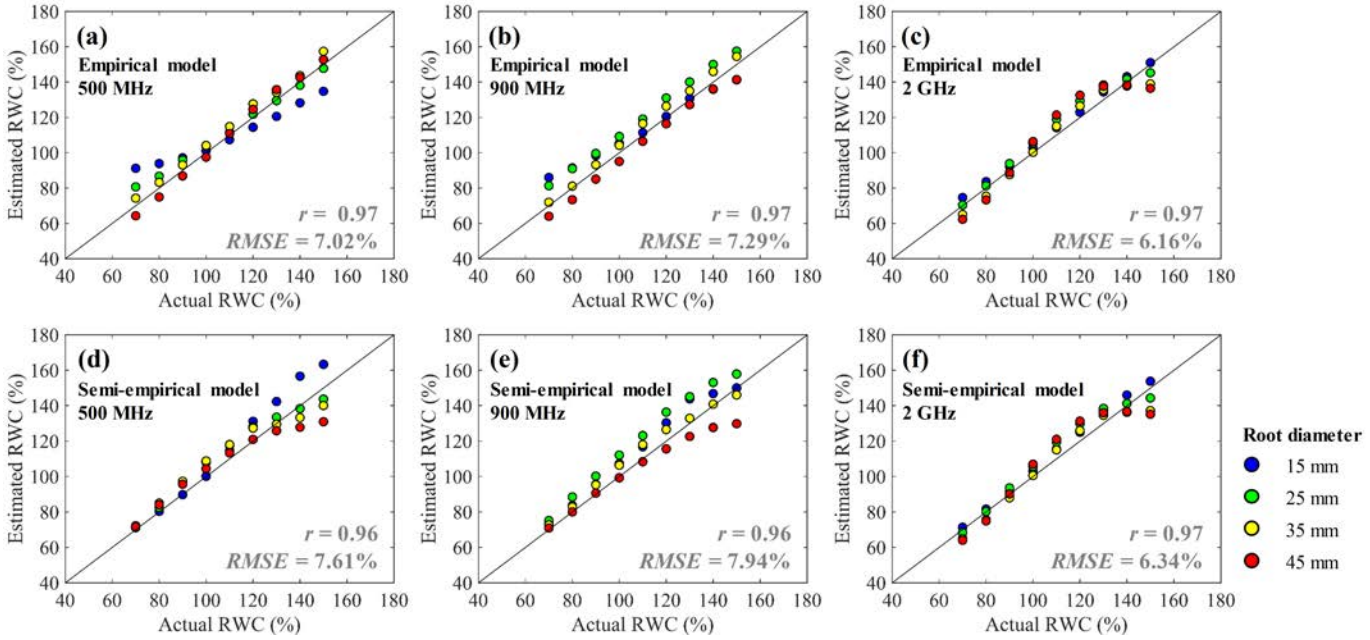

Fig. 7. Comparison of the accuracy of RWC estimation by the (a)–(c) empirical and (d)–(f) semiempirical models for the simulation testing data at different root diameters.

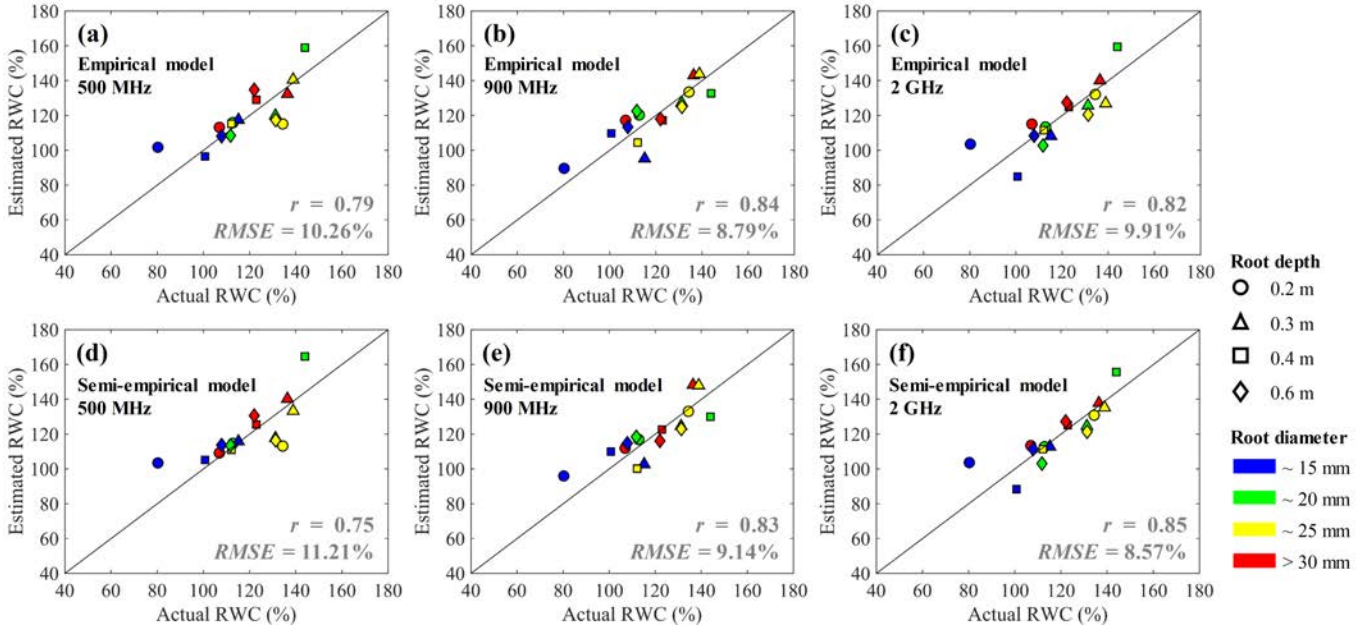

Fig. 8. Comparison of the accuracy of RWC estimation by the (a)–(c) empirical and (d)–(f) semiempirical models for the field data at different root diameters and root depths.

improvements. As the first attempt to relating waveform parameters of root reflections to root parameters, the semiempirical model proposed in this study paves the way for developing more sophisticated physical models to measure other root parameters.

D. Limitations of This Study and Outlook

1) Root samples collected in the study area were limited to a relatively high RWC level, i.e., ranging from 70% to 150%. However, natural living roots exhibit a wider range of RWC [28]. A low RWC cannot create enough contrast in dielectric permittivity with the surrounding soil and leads to a low signal-to-noise ratio of root reflections, which impedes root detection by GPR and the extraction of GPR index [13].
2) The proposed framework was only tested in the homogeneous sandy soil. The setting of roots in the controlled experiments cannot fully represent natural conditions of root growth. In soils with higher heterogeneity, root

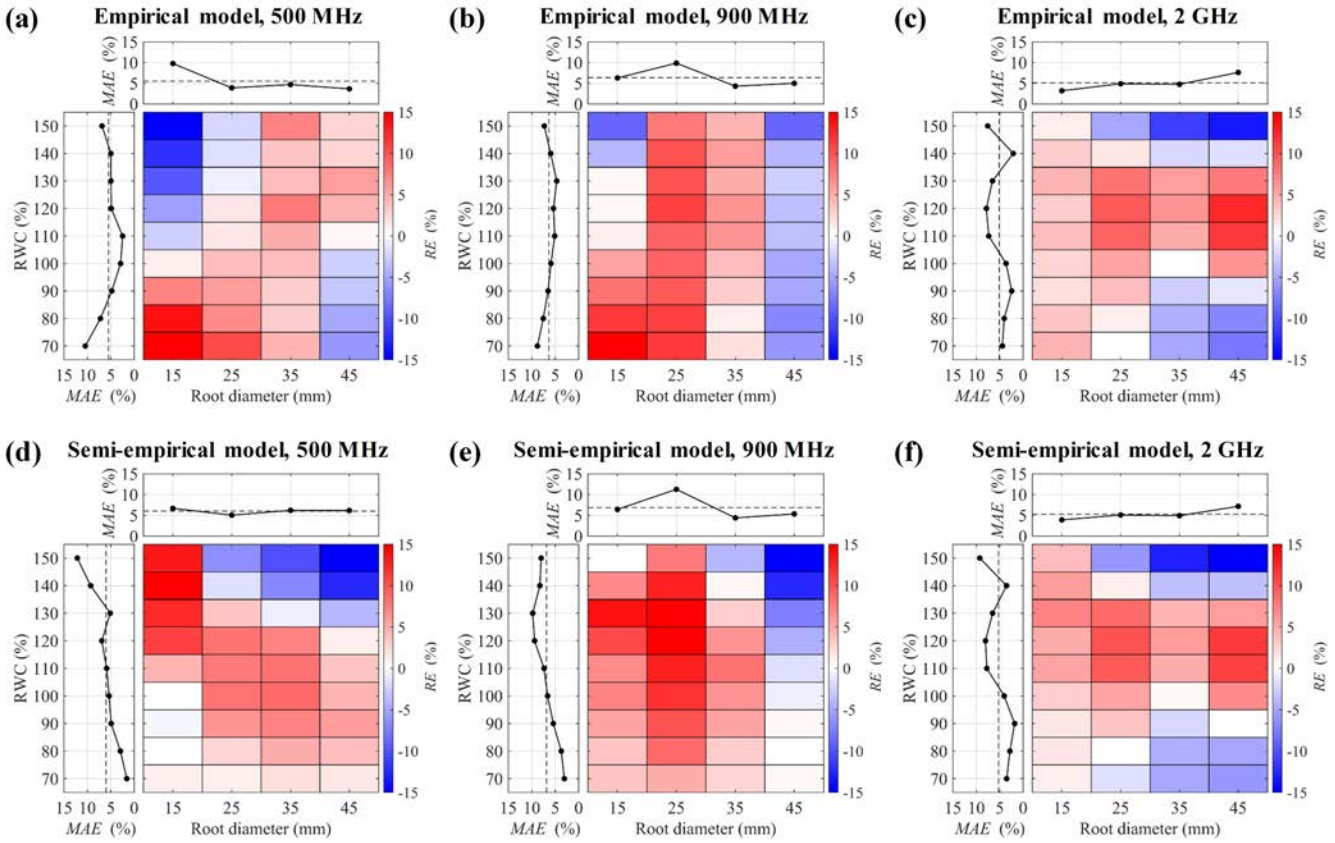

Fig. 9. RE (indicated by blue-red colormap) and MAE (indicated by black solid curves) of RWC estimation by the (a)–(c) empirical model and the (d)–(f) semiempirical model at different levels of RWC and root diameter. The vertical (or horizontal) dashed lines indicate the mean value of MAE at all RWC (or root diameter) levels.

reflections of natural root systems are sometimes not symmetric and complete hyperbolas [32], [41]. This reduces the efficiency of the proposed framework to identify root reflections and estimate RWC. Thus, more field studies are required to test the proposed framework across environments.

3) The proposed GPR-based RWC models are established on the assumption of constant SWC. The signal strength of GPR root reflections is determined by the contrast in dielectric permittivity (or water content) between the root and the surrounding soil [19], [22]. Thus, the parameters of GPR-based RWC models reported here (Table II) are site-specific and need to be calibrated at new field conditions.

To enhance the transferability of the proposed models in different environments, one possibility is to establish more sophisticated physical models that consider the influence of the variation in SWC. The contrast between RWC and SWC can be related to the signal strength per unit root diameter, $1/(a \times D + b) \times S$, through

$$f(\mathrm{RWC} - \mathrm{SWC}) = \frac{S}{a \times D + b} + c \tag{12}$$

where $f(\mathrm{RWC} - \mathrm{SWC})$ is a function of the contrast between RWC and SWC, and c is an unknown parameter representing residual error. Hence, with given values of SWC that are handy to measure in the field, the proposed models can be used to estimate RWC. Most recently, Liu *et al.* [41], [54] developed a novel method of estimating SWC from GPR root reflections without additional auxiliary data. Thus, through computing SWC and optimizing the form of (12), RWC can be calculated by

$$\mathrm{RWC} = f^{-1}\left(\frac{S}{a \times D + b}\right) + \mathrm{SWC} + c. \tag{13}$$

The joint estimation of SWC and RWC by GPR will be examined in follow-up studies.

VII. Conclusion

In Situ quantification of root properties by GPR has gained increasing attention in recent years. This study proposed an automatic processing framework to identify root reflections in GPR images, extract waveform parameters from root reflections, and estimate RWC. Two GPR-based models, one empirical model and one semiempirical model that link RWC to root diameter and the strength of root reflection, were established and validated using GPR data from field-controlled experiments and simulation experiments. Results indicated both models' successful performance in determining RWC at three antenna center frequencies (500 MHz, 900 MHz, and 2 GHz). Regardless of antenna center frequency, the RMSE of RWC estimations for both models was less than 8% for the simulation data and 12% for the field data. Both models

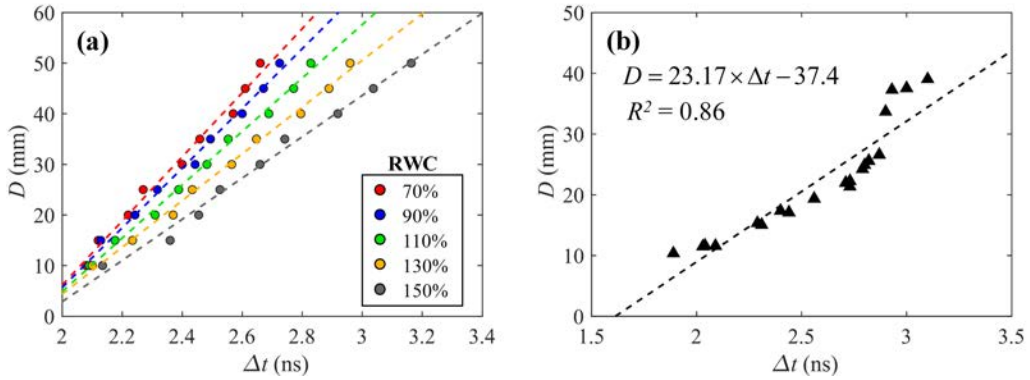

Fig. 10. Strong linear relationship between root diameter (D) and time interval (Δt) extracted from 900-MHz GPR (a) simulation data and (b) field data.

TABLE III

PERFORMANCE OF THE EMPIRICAL MODEL IN MODEL FITTING AND MODEL ESTIMATION FOR GPR DATA COLLECTED WITH DIFFERENT NUMBERS OF ROOT SAMPLES. THE BOLD ITALICIZED NUMBERS REFER TO THE NUMBER OF SAMPLES INVOLVED IN FITTING MODELS

GPR frequency	Model fitting									Model estimation	
	R^2	$R^2_{adjusted}$	F_{value}	f_{value}	S_r	a_1	b_1	c_1	d_1	*RMSE*	r
500 MHz (***16***)	0.76	0.70	8.77	5.59	11.85%	0.07	29.99	-0.02	-28.33	10.26%	0.79
900 MHz (***20***)	0.73	0.68	9.41	5.29	12.43%	0.25	45.22	-0.07	-45.86	11.11%	0.77
2 GHz (***19***)	0.83	0.80	14.8	5.42	10.22%	0.49	52.06	-0.23	-5.68	9.08%	0.83

TABLE IV

PERFORMANCE OF THE SEMIEMPIRICAL MODEL IN MODEL FITTING AND MODEL ESTIMATION FOR GPR DATA COLLECTED WITH DIFFERENT NUMBERS OF ROOT SAMPLES. THE BOLD ITALICIZED NUMBERS REFER TO THE NUMBER OF SAMPLES INVOLVED IN FITTING MODELS

GPR frequency	Model fitting								Model estimation	
	R^2	$R^2_{adjusted}$	F_{value}	f_{value}	S_r	a_2	b_2	c_2	*RMSE*	r
500 MHz (***16***)	0.70	0.66	11.72	6.70	12.43%	17.32	8.33	11.74	11.21%	0.75
900 MHz (***20***)	0.68	0.64	13.00	6.11	12.56%	10.11	-0.34	-8.67	11.58%	0.74
2 GHz (***19***)	0.80	0.78	23.00	6.23	9.28%	82.95	72.20	82.20	8.52%	0.84

achieved the best accuracy in RWC estimation when applied to the 2-GHz data. The proposed framework shows great potential for *in situ* determination of RWC automatically and repeatedly, enhancing GPR's application in ecohydrology. We advocate further field studies under real-world conditions to further test and refine this framework to measure various root parameters by GPR.

APPENDIX

(See Figure 10 and Tables III–IV.)

REFERENCES

[1] R. K. Dixon, A. M. Solomon, S. Brown, R. A. Houghton, M. C. Trexier, and J. Wisniewski, "Carbon pools and flux of global forest ecosystems," *Science*, vol. 263, no. 5144, pp. 185–190, Jan. 1994.

[2] R. A. Gill and R. B. Jackson, "Global patterns of root turnover for terrestrial ecosystems," *New Phytologist*, vol. 147, no. 1, pp. 13–31, Jul. 2000.

[3] P. J. Gregory, *Plant Roots*. Oxford, U.K.: Blackwell, 2006.

[4] J. A. Vrugt, M. T. van Wijk, J. W. Hopmans, and J. Šimunek, "One-, two-, and three-dimensional root water uptake functions for transient modeling," *Water Resour. Res.*, vol. 37, no. 10, pp. 2457–2470, Oct. 2001.

[5] A. Fitter, "Characteristics and functions of roots systems," in *Plant Roots: The Hidden Half*, Y. Waisel, A. Eshel, and U. Kafkafi, Eds., 3rd ed. New York, NY, USA: Marcel Dekker, 2002, pp. 15–32.

[6] J. M. Norman and M. C. Anderson, "Soil-plant-atmosphere continuum," in *Encyclopedia of Soils in the Environment*, vol. 4. Amsterdam, The Netherlands: Elsevier, 2004, pp. 513–521.

[7] H. Chen, M. E. Harmon, R. P. Griffiths, and W. Hicks, "Effects of temperature and moisture on carbon respired from decomposing woody roots," *Forest Ecol. Manage.*, vol. 138, nos. 1–3, pp. 51–64, Nov. 2000.

[8] G. Lobet, V. Couvreur, F. Meunier, M. Javaux, and X. Draye, "Plant water uptake in drying soils," *Plant Physiol.*, vol. 164, no. 4, pp. 1619–1627, Apr. 2014.

[9] Y. Yang, L. Chen, N. Li, and Q. Zhang, "Effect of root moisture content and diameter on root tensile properties," *PLoS ONE*, vol. 11, no. 3, Mar. 2016, Art. no. e0151791.

[10] C. Zhang, X. Zhou, J. Jiang, Y. Wei, J. Ma, and P. D. Hallett, "Root moisture content influence on root tensile tests of herbaceous plants," *Catena*, vol. 172, pp. 140–147, Jan. 2019.

[11] E. Elhacham, L. Ben-Uri, J. Grozovski, Y. M. Bar-On, and R. Milo, "Global human-made mass exceeds all living biomass," *Nature*, vol. 588, no. 7838, pp. 442–444, Dec. 2020.

[12] A. Aboudourib, M. Serhir, and D. Lesselier, "A processing framework for tree-root reconstruction using ground-penetrating radar under heterogeneous soil conditions," *IEEE Trans. Geosci. Remote Sens.*, vol. 59, no. 1, pp. 208–219, Jan. 2021.

[13] Y. Hirano *et al.*, "Limiting factors in the detection of tree roots using ground-penetrating radar," *Plant Soil*, vol. 319, nos. 1–2, pp. 15–24, Jun. 2009.

[14] D. A. Robinson *et al.*, "Advancing process-based watershed hydrological research using near-surface geophysics: A vision for, and review of, electrical and magnetic geophysical methods," *Hydrological Processes*, vol. 22, no. 18, pp. 3604–3635, Aug. 2008.

[15] X. Liu, J. Chen, X. Cui, Q. Liu, X. Cao, and X. Chen, "Measurement of soil water content using ground-penetrating radar: A review of current methods," *Int. J. Digit. Earth*, vol. 12, no. 1, pp. 95–118, Jan. 2019.

[16] B. Fan *et al.*, "Exploring the interplay between infiltration dynamics and critical zone structures with multiscale geophysical imaging: A review," *Geoderma*, vol. 374, Sep. 2020, Art. no. 114431.

[17] J. Hruska, J. Cermak, and S. Sustek, "Mapping tree root systems with ground-penetrating radar," *Tree Physiol.*, vol. 19, no. 2, pp. 125–130, Feb. 1999.

[18] A. M. Alani and L. Lantini, "Recent advances in tree root mapping and assessment using non-destructive testing methods: A focus on ground penetrating radar," *Surv. Geophys.*, vol. 41, no. 3, pp. 605–646, May 2020.

[19] L. Guo, J. Chen, X. Cui, B. Fan, and H. Lin, "Application of ground penetrating radar for coarse root detection and quantification: A review," *Plant Soil*, vol. 362, nos. 1–2, pp. 1–23, Jan. 2013.

[20] Y. Wu, L. Guo, X. Cui, J. Chen, X. Cao, and H. Lin, "Ground-penetrating radar-based automatic reconstruction of three-dimensional coarse root system architecture," *Plant Soil*, vol. 383, nos. 1–2, pp. 155–172, Oct. 2014.

[21] D. B. Stover, F. P. Day, J. R. Butnor, and B. G. Drake, "Effect of elevated CO_2 on coarse-root biomass in Florida scrub detected by ground-penetrating radar," *Ecology*, vol. 88, no. 5, pp. 1328–1334, 2007.

[22] C. V. M. Barton and K. D. Montagu, "Detection of tree roots and determination of root diameters by ground penetrating radar under optimal conditions," *Tree Physiol.*, vol. 24, no. 12, pp. 1323–1331, Dec. 2004.

[23] J. R. Butnor, J. A. Doolittle, K. H. Johnsen, L. Samuelson, T. Stokes, and L. Kress, "Utility of ground-penetrating radar as a root biomass survey tool in forest systems," *Soil Sci. Soc. Amer. J.*, vol. 67, no. 5, pp. 1607–1615, Sep. 2003.

[24] M. Molon, J. I. Boyce, and M. A. Arain, "Quantitative, nondestructive estimates of coarse root biomass in a temperate pine forest using 3-D ground-penetrating radar (GPR)," *J. Geophys. Res. Biogeosci.*, vol. 122, no. 1, pp. 80–102, Jan. 2017.

[25] J. R. Butnor, J. A. Doolittle, L. Kress, S. Cohen, and K. H. Johnsen, "Use of ground-penetrating radar to study tree roots in the Southeastern United States," *Tree Physiol.*, vol. 21, no. 17, pp. 1269–1278, 2001.

[26] M. Dannoura *et al.*, "Detection of *Cryptomeria japonica* roots with ground penetrating radar," *Plant Biosyst.*, vol. 142, no. 2, pp. 375–380, Jul. 2008.

[27] X. Cui, L. Guo, J. Chen, X. Chen, and X. Zhu, "Estimating tree-root biomass in different depths using ground-penetrating radar: Evidence from a controlled experiment," *IEEE Trans. Geosci. Remote Sens.*, vol. 51, no. 6, pp. 3410–3423, Jun. 2013.

[28] L. Guo, H. Lin, B. Fan, X. Cui, and J. Chen, "Impact of root water content on root biomass estimation using ground penetrating radar: Evidence from forward simulations and field controlled experiments," *Plant Soil*, vol. 371, nos. 1–2, pp. 503–520, Oct. 2013.

[29] L. Guo, H. Lin, B. Fan, X. Cui, and J. Chen, "Forward simulation of root's ground penetrating radar signal: Simulator development and validation," *Plant Soil*, vol. 372, nos. 1–2, pp. 487–505, Nov. 2013.

[30] A. Paz, E. Thorin, and C. Topp, "Dielectric mixing models for water content determination in woody biomass," *Wood Sci. Technol.*, vol. 45, no. 2, pp. 249–259, May 2011.

[31] S. A. Al Hagrey, "Geophysical imaging of root-zone, trunk, and moisture heterogeneity," *J. Experim. Botany*, vol. 58, no. 4, pp. 839–854, Mar. 2007.

[32] W. Li, X. Cui, L. Guo, J. Chen, X. Chen, and X. Cao, "Tree root automatic recognition in ground penetrating radar profiles based on randomized Hough transform," *Remote Sens.*, vol. 8, no. 5, p. 430, May 2016.

[33] S. Zhu, C. Huang, Y. Su, and M. Sato, "3D ground penetrating radar to detect tree roots and estimate root biomass in the field," *Remote Sens.*, vol. 6, no. 6, pp. 5754–5773, Jun. 2014.

[34] G. Hans, D. Redman, B. Leblon, J. Nader, and A. La Rocque, "Determination of log moisture content using early-time ground penetrating radar signal," *Wood Mater. Sci. Eng.*, vol. 10, no. 1, pp. 112–129, Jan. 2015.

[35] G. Hans, D. Redman, B. Leblon, J. Nader, and A. L. Rocque, "Determination of log moisture content using ground penetrating radar (GPR). Part 1. Partial least squares (PLS) method," *Holzforschung*, vol. 69, no. 9, pp. 1117–1123, Nov. 2015.

[36] W. Li, J. Wen, Z. Xiao, and S. Xu, "Application of ground-penetrating radar for detecting internal anomalies in tree trunks with irregular contours," *Sensors*, vol. 18, no. 2, p. 649, Feb. 2018.

[37] I. Giannakis, F. Tosti, L. Lantini, and A. M. Alani, "Health monitoring of tree trunks using ground penetrating radar," *IEEE Trans. Geosci. Remote Sens.*, vol. 57, no. 10, pp. 8317–8326, Oct. 2019.

[38] C. Lv *et al.*, "Fluvial response to precipitation variations since 36 ka in the Hunshandake Sandy Land in North China," *Geomorphology*, vol. 317, pp. 128–138, Sep. 2018.

[39] X. Yang *et al.*, "Initiation and variation of the dune fields in semi-arid China—With a special reference to the hunshandake sandy land, inner mongolia," *Quaternary Sci. Rev.*, vol. 78, pp. 369–380, Oct. 2013.

[40] A. Giannopoulos, "Modelling ground penetrating radar by GprMax," *Construct. Building Mater.*, vol. 19, no. 10, pp. 755–762, Dec. 2005.

[41] X. Liu *et al.*, "Non-invasive estimation of root zone soil moisture from coarse root reflections in ground-penetrating radar images," *Plant Soil*, vol. 436, nos. 1–2, pp. 623–639, Mar. 2019.

[42] Q. Liu, X. Cui, X. Liu, J. Chen, X. Chen, and X. Cao, "Detection of root orientation using ground-penetrating radar," *IEEE Trans. Geosci. Remote Sens.*, vol. 56, no. 1, pp. 93–104, Jan. 2018.

[43] A. E. Mihai, A. G. Gerea, G. Curioni, P. Atkins, and F. Hayati, "Direct measurements of tree root relative permittivity for the aid of GPR forward models and site surveys," *Near Surf. Geophys.*, vol. 17, no. 3, pp. 299–310, Jun. 2019.

[44] G. C. Topp, J. L. Davis, and A. P. Annan, "Electromagnetic determination of soil water content: Measurements in coaxial transmission lines," *Water Resour. Res.*, vol. 16, no. 3, pp. 574–582, Jun. 1980.

[45] N. Cassidy, "Ground penetrating radar data processing, modelling and analysis," in *Ground Penetrating Radar Theory and Applications*. Amsterdam, The Netherlands: Elsevier, 2009, pp. 141–176.

[46] A. Delgado *et al.*, "Ground penetrating radar: A case study for estimating root bulking rate in cassava (Manihot esculenta Crantz)," *Plant Methods*, vol. 13, no. 1, p. 65, Aug. 2017.

[47] L. Xu, "Randomized Hough transform (RHT): Basic mechanisms, algorithms, and computational complexities," *Comput. Vis. Image Understand.*, vol. 57, no. 2, pp. 131–154, Mar. 1993.

[48] A. Simi, S. Bracciali, and G. Manacorda, "Hough transform based automatic pipe detection for array GPR: Algorithm development and on-site tests," in *Proc. IEEE Radar Conf.*, May 2008, pp. 1–6.

[49] Y. Hirano *et al.*, "Detection frequency of *Pinus thunbergii* roots by ground-penetrating radar is related to root biomass," *Plant Soil*, vol. 360, nos. 1–2, pp. 363–373, Nov. 2012.
[50] J. Bain, F. Day, and J. Butnor, "Experimental evaluation of several key factors affecting root biomass estimation by 1500 NHz ground-penetrating radar," *Remote Sens.*, vol. 9, no. 12, p. 1337, Dec. 2017.
[51] X. Cui, J. Chen, J. Shen, X. Cao, X. Chen, and X. Zhu, "Modeling tree root diameter and biomass by ground-penetrating radar," *Sci. China Earth Sci.*, vol. 54, no. 5, pp. 711–719, May 2011.
[52] C. D. Orme and T. Yamagata, "The asymptotic distribution of the F-test statistic for individual effects," *Econometrics J.*, vol. 9, no. 3, pp. 404–422, Nov. 2006.
[53] X. Cui *et al.*, "Pairing dual-frequency GPR in summer and winter enhances the detection and mapping of coarse roots in the semi-arid Shrubland in China," *Eur. J. Soil Sci.*, vol. 71, no. 2, pp. 236–251, Mar. 2020.
[54] X. Liu *et al.*, "Noninvasive 2D and 3D mapping of root zone soil moisture through the detection of coarse roots with ground-penetrating radar," *Water Resour. Res.*, vol. 56, no. 5, pp. 1–24, May 2020.
[55] J. R. Butnor, L. J. Samuelson, T. A. Stokes, K. H. Johnsen, P. H. Anderson, and C. A. González-Benecke, "Surface-based GPR underestimates below-stump root biomass," *Plant Soil*, vol. 402, nos. 1–2, pp. 47–62, May 2016.
[56] L. J. Samuelson *et al.*, "Ecosystem carbon density and allocation across a chronosequence of longleaf pine forests," *Ecological Appl.*, vol. 27, no. 1, pp. 244–259, Jan. 2017.
[57] X. Xu, W. Gao, D. Zhang, T. Li, and X. Qiao, "Cloud-based difference algorithm using big GPR data for roadbed damage detection," *Concurrency Comput. Pract. Exper.*, vol. 32, no. 23, Nov. 2019.
[58] J. Hirte, J. Leifeld, S. Abiven, H.-R. Oberholzer, A. Hammelehle, and J. Mayer, "Overestimation of crop root biomass in field experiments due to extraneous organic matter," *Frontiers Plant Sci.*, vol. 8, p. 284, Mar. 2017.
[59] A. Gábor and J. R. Banga, "Robust and efficient parameter estimation in dynamic models of biological systems," *BMC Syst. Biol.*, vol. 9, no. 1, pp. 1–25, Oct. 2015.